Doping Engineering Enables Highly Conductive and Thermally Stable n-Type Organic Thermoelectrics with High Power Factor

Liu, Jian; Garman, Matt P.; Dong, Jingjin; van der Zee, Bas; Qiu, Li; Portale, Giuseppe; Hummelen, Jan C.; Koster, L. Jan Anton

Published in:
ACS Applied Energy Materials

DOI:
10.1021/acsaem.9b01179

Publication date:
2019

ACS APPLIED ENERGY MATERIALS

Article

Cite This: ACS Appl. Energy Mater. 2019, 2, 6664−6671

www.acsaem.org

Doping Engineering Enables Highly Conductive and Thermally Stable n-Type Organic Thermoelectrics with High Power Factor

Jian Liu,*[,†] Matt P. Garman,[†] Jingjin Dong,[†] Bas van der Zee,[†] Li Qiu,[†,‡] Giuseppe Portale,[†] Jan C. Hummelen,[†,‡] and L. Jan Anton Koster*[,†]

[†]Zernike Institute for Advanced Materials, Nijenborgh 4, NL-9747 AG Groningen, The Netherlands

[‡]Stratingh Institute for Chemistry, Nijenborgh 4, NL-9747 AG Groningen, The Netherlands

Supporting Information

ABSTRACT: This work exploits the scope of doping engineering as an enabler for better-performing and thermally stable n-type organic thermoelectrics. A fullerene derivative with polar triethylene glycol type side chain (PTEG-1) is doped either by "coprocessing doping" with n-type dopants such as n-DMBI and TBAF or by "sequential doping" through thermal deposition of Cs_2CO_3. Solid-state diffusion of Cs_2CO_3 appears to dope PTEG-1 in the strongest manner, leading to the highest electrical conductivity of ∼7.5 S/cm and power factor of 32 μW/(m K^2). Moreover, the behavior of differently doped PTEG-1 films under thermal stress is examined by electric and spectroscopic means. Cs_2CO_3-doped films are most stable, likely due to a coordinating interaction between the polar side chain and Cs^+-based species, which immobilizes the dopant. The high power factor and good thermal stability of Cs_2CO_3-doped PTEG-1 make it very promising for tangible thermoelectric applications.

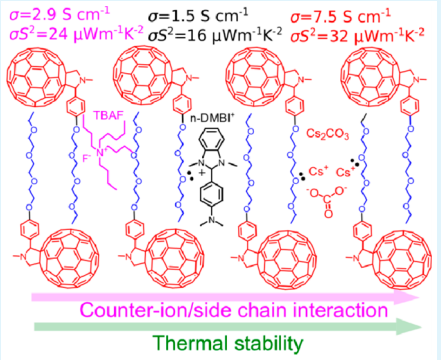

KEYWORDS: *doping engineering, electrical conductivity, power factor, thermal stability, fullerene derivative*

1. INTRODUCTION

Recently, the prospect of realizing lightweight, economical, and mechanically flexible electricity generation modules has led to increased activity in research concerning organic thermoelectric (TE) materials.[1−5] The performance of a TE material is expressed by a dimensionless figure of merit, $ZT = S^2\sigma T/\kappa$, where S, σ, κ, and T are the Seebeck coefficient, electrical conductivity, thermal conductivity, and absolute temperature, respectively.[4] In an organic material, molecules interact with each other through a weak van der Waals force, enabling a poorly thermally conductive system with low thermal conductivity of <1 W/(m K). As such, their TE performances are determined by a parameter known as the power factor (PF):[6,7] $PF = S^2\sigma$. Tangible TE applications require both p- and n-type conducting materials with high power factors and sufficient working stability under a thermal stress. However, the latter is still much less developed than the former.[8−15] In this regard, growing research efforts turn to design better n-type TE systems.

Aiming at optimizing the power factor of an n-type TE system, a tunable number of free charges are enabled by doping through electron transfer from n-dopant to host material. Adachi and co-workers reported an evaporated C_{60}/cesium carbonate (Cs_2CO_3) bilayer, which offers a σ of ∼8 S/cm and a $S^2\sigma$ of ∼20.5 μW/(m K^2).[16] However, with a few exceptions,[8,17−21] most n-doped solution-processed organic systems exhibit a σ of <1 S/cm and a $S^2\sigma$ of <10 μW/(m K^2).[22−24] For instance, Chabinyc and co-workers reported a σ of ∼10^{-3} S/cm and a $S^2\sigma$ of ∼0.1 μW/(m K^2) for a doped naphthalenediimide (NDI)-based copolymer by a 1*H*-benzoimidazole derivative (n-DMBI).[11] Afterward, considerable effort has been directed to enhance the n-doping efficiency of NDI-based copolymers by improving the host/dopant miscibility,[25−28] planarizing the backbone,[23,29] and tailoring the density of states.[24] Particularly, the polar side chains have been used by us and other researchers to improve the system miscibility and thus the electrical conductivity.[20,27,30−32] This led to a σ of 0.3 S/cm and $S^2\sigma$ of 0.4 μW/(m K^2) for conjugated polymers and ∼2 S/cm and 16.7 μW/(m K^2) for fullerene derivatives.[20,33] Alternatively, Yee and co-workers reported an n-type nickel ethene tetrathiolate (NiETT) polymer-based composite, which shows a σ of >1 S/cm and a $S^2\sigma$ of >10 μW/(m K^2).[34] Most of the previous works focused on developing better host materials while how to choose an n-type dopant and the doping method are rarely explored. Moreover, it is unknown whether or not those previously reported n-doped organic systems can withstand a thermal stress in an operating model. Very recently, Kemerink and co-workers reported an "inverse-sequential" doping method for a fullerene derivative, which offers ∼6 times higher σ and $S^2\sigma$ compared to the traditional "coprocessing" (directly alloying the host and dopant in solid).[35] This study

Received: June 14, 2019
Accepted: August 19, 2019
Published: August 19, 2019

DOI: 10.1021/acsaem.9b01179
ACS Appl. Energy Mater. 2019, 2, 6664−6671

undercores the significance of the doping method for n-type organic thermoelectrics.

Here, we explored the impact of different doping methods not only on the performance but also on the thermal stability of n-type organic thermoelectrics. This is a case study of a fullerene derivative with a polar triethylene glycol-type side chain (PTEG-1). PTEG-1 was doped either by blending with an n-type dopant (n-DMBI or TBAF) or by solid-state diffusion of inorganic salts like Cs_2CO_3. Cs_2CO_3 was found to be the most effective dopant for PTEG-1, giving the highest σ of ~7.5 S/cm. Doping PTEG-1 with TBAF and n-DMBI gave the optimized σ of 3.2 and 2 S/cm, respectively. Finally, PTEG-1 films doped by n-DMBI, TBAF, and Cs_2CO_3 showed optimized $S^2\sigma$ of 16, 24, and 32 μW/(m K^2), respectively. These values put them among the best performing n-type organic thermoelectrics. Additionally, the different doping methods led to a variation in film density, which appears to dictate the thermal stability of the doped films. Doping with Cs_2CO_3 yielded the most stable films. Our study offers an insight into the effect of doping methods on the thermoelectric performance and the thermal stability of doped films.

2. RESULTS AND DISCUSSION

2.1. Doping Engineering and Electrical Conductivity. Figure 1 shows the chemical structures of host and dopants as

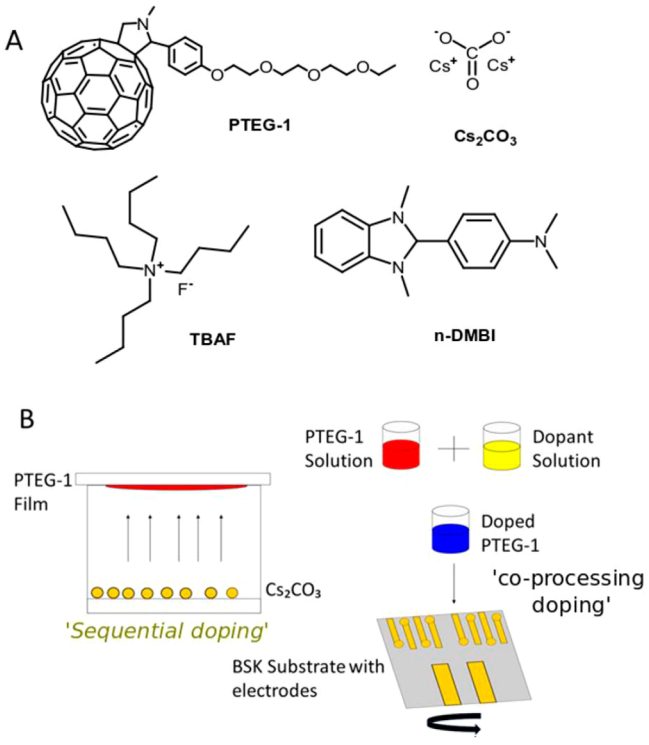

Figure 1. (A) Chemical structures of the host (PTEG-1) and the dopants (TBAF, n-DMBI, and Cs_2CO_3). (B) Schematic of the doping processes ("sequential doping" and "coprocessing doping").

well as the corresponding schematic doping processes. Previous studies indicated that PTEG-1 can be effectively doped by n-DMBI.[20,36] Although Cs_2CO_3 and TABF have proven effective dopants for fullerene-based materals such as C_{60} and PCBM,[16,37] they have not been used to dope PTEG-1, and the corresponding effects on the relevant n-type thermoelectrics are yet to be reported. Similar to the doping process with n-DMBI, TBAF was mixed with PTEG-1 in chloroform, and the mixture was used to prepare the doped PTEG-1 film in a one-step process. This process is known as "coprocessing doping". Alternatively, PTEG-1 was doped by the inorganic salt Cs_2CO_3 in a two-step process, in which the inorganic salt was thermally deposited on top of solution-cast neat PTEG-1 film. We refer to this process as "sequential doping". Earlier studies on Cs_2CO_3 indicated that Cs_2CO_3 decomposes into cesium oxide during thermal evaporation.[38] In this study, the Cs_2CO_3 decomposition was evidenced by gasing during the evaporation process. Therefore, the real dopant may be cesium oxide instead of Cs_2CO_3. However, as this work is not focused on the doping mechanism; for simplicity, we still refer to this as "Cs_2CO_3 doping". It is speculated that Cs_2CO_3 (or a resulting species) diffuses into the bulk of the host film and enables the n-doping process.

Figure 2 displays the electrical conductivity of doped PTEG-1 films after three different doping processes and measured by a standard four-point probe method (see the details in the Experimental Section). The neat PTEG-1 film exhibited a very low σ of 10^{-9} S/cm. As shown in Figure 2A, the electrical conductivity of the PTEG-1 films greatly increased upon blending with n-DMBI and TBAF. The doped PTEG-1 films exhibited a peak σ of 2 and 3.2 S/cm at a doping concentration of 3 wt % for n-DMBI and 5 wt % for TBAF, respectively. By further increasing the dopant loading, the electrical conductivity dropped in both cases, likely because the high concentration of dopant molecules disrupted the film microstructure.[18] Figure 2B shows the electrical conductivity of PTEG-1 films doped by "sequential doping" with evaporated Cs_2CO_3. It should be pointed out that it is very difficult to determine how much of the deposited Cs_2CO_3 really diffuses into the active layer to n-dope the material. However, by controlling the Cs_2CO_3 thickness, it is possible to qualitatively modulate the amount of Cs_2CO_3 diffusing into the active layer. By increasing the thickness of the Cs_2CO_3 layer, the electrical conductivity increased to a peak at 8 nm and then decreased. A best σ of ~7.5 S/cm was achieved, representing the highest value for n-doped fullerene derivatives. One may have a concern regarding whether ion movement contributes to the charge transport in doped films with salts such as TBAF and Cs_2CO_3. To have an insight into this point, we performed several sets of experiments to examine the possible ionic behavior, and the results are displayed in Figure S1 of the Supporting Information. The results indicate that for the doped PTEG-1 films with salts ions hardly move within the bias range used in this study, and capacitive behavior was not apparently seen. As such, we believe that the ionic transport is negligible in our doped organic systems.

2.2. Molecular Packing. The microstructure of various PTEG-1-based films was investigated by two-dimensional (2D) grazing incidence wide-angle X-ray scattering (GIWAXS). The corresponding 2D-GIWAXS patterns and linecuts are shown in Figure 3. Four strong scattering peaks are clearly seen along the near out-of-plane q_z direction for neat PTEG-1 film (Figure 3A). These signals are attributed to the (00l) family of reflections, suggesting that PTEG-1 packs into a layered structure parrallel to the substrate. The layer planes contain the buckyball and the glycolated side chain. The (001) peak position for the neat PTEG-1 thin film determines a spacing of 2.25 nm. The $\pi-\pi$ stacking peak of fullerene cages along the in-plane direction is at q_r = 1.23 Å^{-1}, which corresponds to a spacing of 0.51 nm. These results are in line

DOI: 10.1021/acsaem.9b01179
ACS Appl. Energy Mater. 2019, 2, 6664−6671

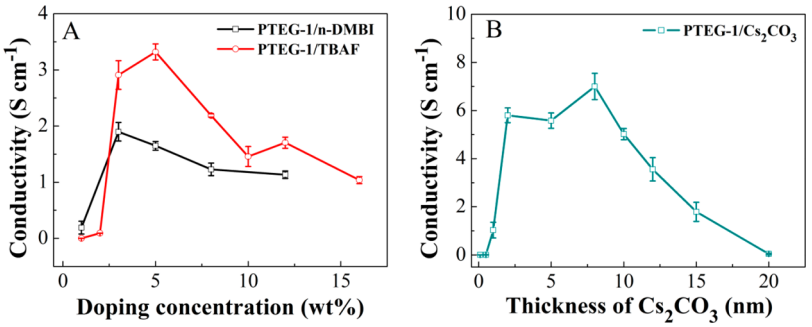

Figure 2. n-doping PTEG-1 with different dopants. (A) plots of electrical conductivity versus doping concentration in the doped PTEG-1 by n-DMBI and TBAF. (B) electrical conductivity as a function of thickness of Cs_2CO_3 layer.

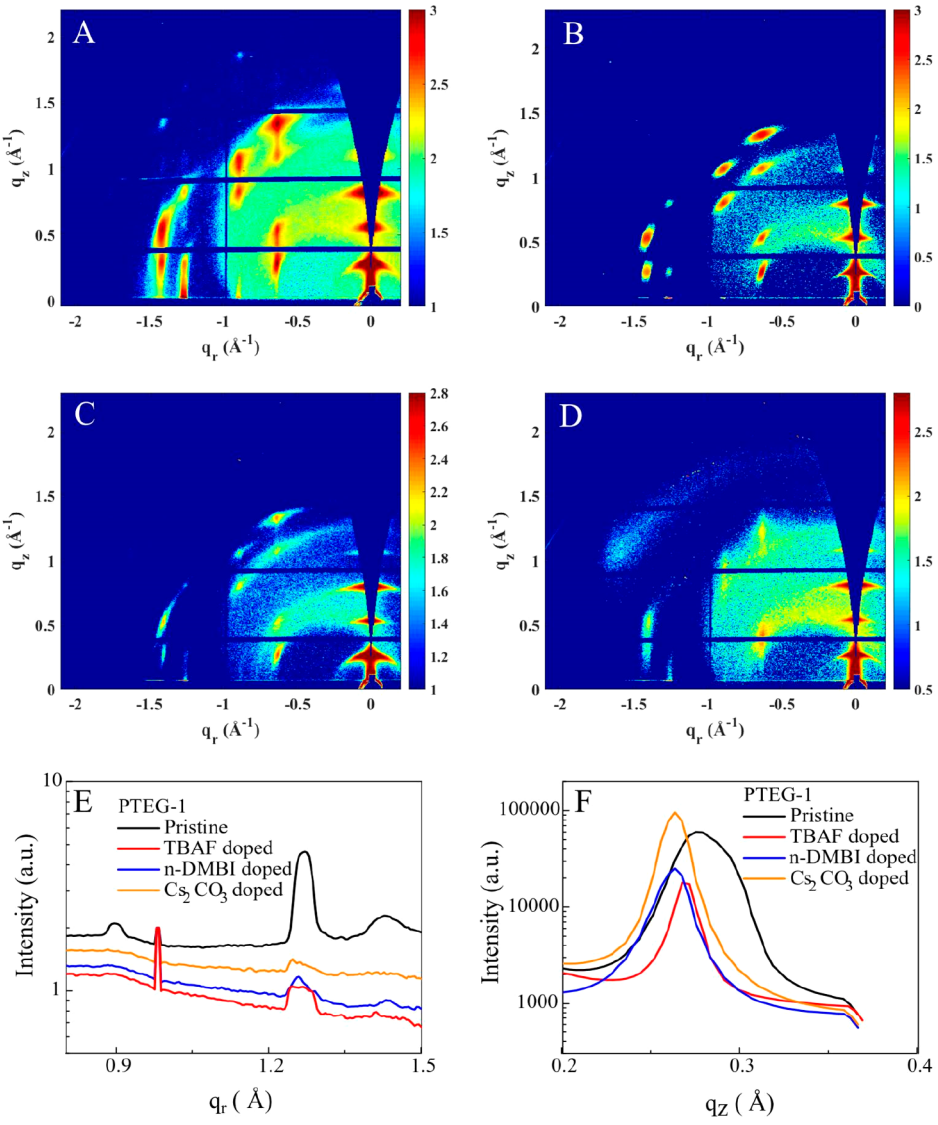

Figure 3. 2D GIWAXS patterns of neat PTEG-1 (A) and doped PTEG-1 films with TBAF (B), n-DMB (C), and Cs_2CO_3 (D) and their corresponding linecuts (E) in the in-plane direction and (F) in the out-of-plane direction.

with our previous report.[20] The doping processes appear to not change the orientation of PTEG-1 molecules and π-stacking spacing (Figure 3B–F). However, the q_z (001) peak shifts to larger spacings, depending on the doping process. For doped PTEG-1 films by coprocessing with n-DMBI and TBAF, the (001) spacing is shifted to 2.40 nm, while for "sequential doping" with Cs_2CO_3 it shifted to 2.33 nm. On the basis of these observations, we assume that the dopants are mainly located in the plane of the polar side chains, and the different (001) spacings are caused by the varying sizes of the dopants. However, it is unclear whether or not the dopants were also incorporated in the amorphous regions. The crystallinity of PTEG-1 film was reduced more upon Cs_2CO_3 doping than in the case of "coprocessing doping". The reason behind is still

DOI: 10.1021/acsaem.9b01179
ACS Appl. Energy Mater. 2019, 2, 6664–6671

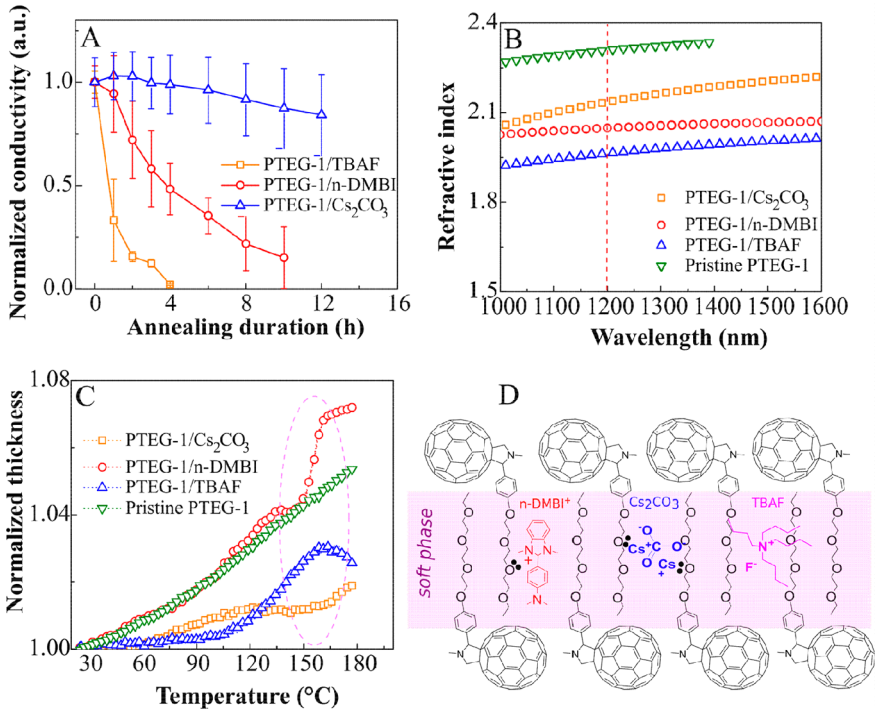

Figure 4. Thermal stability of PTEG-1-based films doped by various dopants. (A) Degradation of electrical conductivities in doped PTEG-1 films with three dopants (TBAF, n-DMBI, and Cs_2CO_3) upon thermal stress (150 °C). (B) Refractive index n spectra of various PTEG-1-based thin films. (C) In situ (normalized) thickness evolution of various PTEG-1-based films with growing temperature detected in dynamic ellipsometry model. (D) Schematic of the interaction between the dopants and host (the doping mechanism is not fully demonstrated).

unknown, and we surmise that it is correlated to the polar side chain and the unique molecular stacking of PTEG-1.

2.3. Electric and Spectroscopic Characterization of Stability under a Thermal Stress. The operating stability of doped organic films under a thermal stress is very critical to practical thermoelectric applications. As such, the dopant should be carefully selected, with regard to both the thermoelectric performance and thermal stability of the TE film. Figure 4A displays the evolution of the electrical conductivity of doped PTEG-1 films upon heating at 150 °C for different durations in an inert atmosphere. The PTEG-1 film doped with Cs_2CO_3 ("sequential doping") proved most stable and maintained 80% of its initial electrical conductivity after thermal annealing for 12 h. In contrast, the PTEG-1 films doped by "coprocessing doping" showed a much faster decrease in electrical conductivity. The TBAF-doped PTEG-1 film completely lost its electrical conductivity after 4 h while the n-DMBI-doped PTEG-1 film degraded to 5% of its initial conductivity. Previous studies attributed such a loss of electrical conductivity to a dedoping process, which is related to the diffusion of dopant molecules out of the host matrix upon the thermal annealing.[20,39] In this sense, an improved thermal stability may indicate less thermal annealing-driven spacial mobility of the dopant molecules.

Incorporating extrinsic dopants into a host matrix is expected to modify the molecular packing and thus the density (ρ) and polarizability of the film. The variations in film density and polarizability reflect into changes in the refractive index (n).[40,41] As the molecular orientation of PTEG-1 is not affected by the doping process (as indicated by GIWAXS data), the refractive index is mainly a function of the film density. In the region of the spectrum where PTEG-1 does not absorb, the variation in refractive index can be expressed as[40]

$$\frac{n_t^2 - 1}{n_0^2 - 1} \cong \frac{\rho_t}{\rho_0} \quad (1)$$

Clearly, a larger refractive index corresponds to a higher density of the film. The UV−vis−NIR absorption spectra of various PTEG-1-based films were measured to determine the transparency in the region of 1000−1700 nm (Figure S2). We measured the refractive index (n) of various PTEG-1-based films in such a spectral region by noninvasive variable angle ellipsometry (see Figure 4B). The neat PTEG-1 film displays the highest refractive index n = 2.3 (at 1200 nm) and is therefore assigned as being the most dense film. Upon doping, n decreases, indicating that the films become less dense. The order of the density of the PTEG-1 films is neat > Cs_2CO_3-doped > n-DMBI-doped > TBAF-doped. The dedoping process upon thermal annealing is considered to be related to the diffusion of dopant and the resultant demixing of the host and dopant.[31,39] If the doped PTEG-1 film is more closely packed, there is less space for dopant molecules to diffuse, which may lead to a better thermal stability. In this way, the density of doped PTEG-1 film explains the variation of thermal stability shown in Figure 4A.

Variable temperature ellipsometry is a powerful tool to detect the real-time phase behavior of organic films via examining the thickness variation with temperature.[40,41] Figure 4C displays the evolution of thickness of the PTEG-1-based films with temperature (25−180 °C), measured by variable temperature ellipsometry in an inert atmosphere. At temperatures above 150 °C, the doped PTEG-1 films by TBAF and n-DMBI showed a fast change in thickness with elevating temperature, attributing to the demixing of the host and dopant molecules. In contrast, the PTEG-1 film doped with Cs_2CO_3 displayed a plateau with the slowest change in the

DOI: 10.1021/acsaem.9b01179
ACS Appl. Energy Mater. 2019, 2, 6664−6671

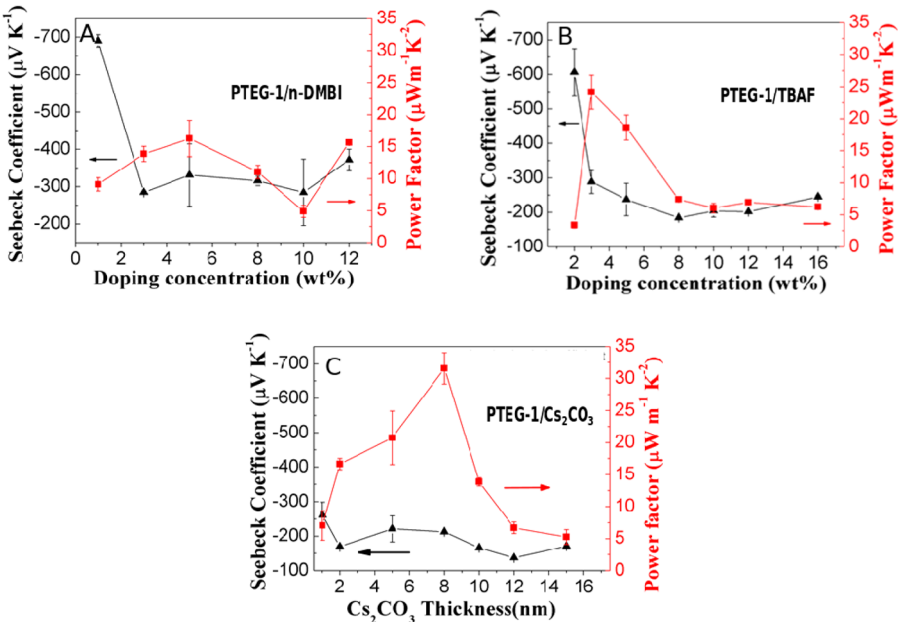

Figure 5. Thermoelectric parameters (S and $S^2\sigma$) plots for PTEG-1-based films doped by n-DMBI (A), TBAF (B), and Cs_2CO_3 (C).

Table 1. List of Thermoelectric Parameters of Solution-Based n-Type OTEs

host	dopant (method)	conductivity [S/cm]	Seebeck coefficient [μV/K]	power factor [μW/(m K^2)]	ref
PTEG-1	Cs_2CO_3 (evaporate)	7.5	−212	32	this work
PTEG-1	n-DMBI (solution)	1.5	−330	16	this work
PTEG-1	TBAF (solution)	2.9	−288	24	this work
C_{60}	Cs_2CO_3 (evaporate)	8	−160	20	16
PTeEG-1	n-DMBI (solution)	2.3	−319	23	18
A-DCV-DPPTT	n-DMBI (solution)	3.1	−568	105	8
TEG-N2200	n-DMBI (solution)	0.17	−153	0.4	27
p(gNDI-gT2)	n-DMBI (solution)	0.3	−93	0.4	28
FBDPPV	n-DMBI (solution)	14	−140	28	21
PNDTI-BBT-DP	n-DMBI (solution)	5	−169	14	17
PNDI2TEG-2Tz	n-DMBI (solution)	1.8	−159	4.6	24
P(NDI2OD-Tz2)	TDAE (vapor)	0.06	−447	1.5	23
PDPF	n-DMBI (solution)	1.3	−235	4.7	19

thickness. These results explain the thermal stability characteristics of PTEG-1 films doped by various dopants, which is related to the demixing of the host and dopant molecules driven by the thermal stress. As mentioned above, the (cationic) dopants are expected to be mainly incorporated in the plane of the polar side chains. This allows us to discuss the microstructural origin of the different behaviors of the doped films under thermal stress. It has been well established that the ethylene oxide-based organic species can chelate alkali salts by forming a complex with the cationic species through interaction with the lone pairs of the oxygen atoms of the ether linkages.[42,43] This parallels the famous and quite strong crown ether−cation interactions. We postulate that the triethylene glycol type side chain may, to some extent, stabilize Cs_2CO_3 (or resulting cationic dopant species) and thus make it less mobile under thermal stress as illustrated in Figure 4D. Hence, the Cs_2CO_3-doped PTEG-1 film exhibits the best thermal stability in this study. As for the case of TBAF doping, the counterion TBA^+ possesses the most bulky structure and therefore is expected to has weakest interaction with the surroundings composed by the glycolated side chains. As such, the PTEG-1-based film doped by TBAF renders the worst stability under a thermal stress.

2.4. Thermoelectric Performance. The energy offset between the Fermi level energy (E_F) and the charge transport energy (E_T) governs the Seebeck coefficient.[24,44] By furthering the doping, more charge carriers are produced, causing a shift of E_F toward E_T and a decrease in the absolute S value. As such, S can be used to indirectly evaluate the doping level. We measured S values of PTEG-1 films doped with the three different dopants and calculated the power factors accordingly, which are displayed in Figure 5A−C. All of the doped PTEG-1 films show negative S, indicating the electron as the dominating mobile charge carrier. The PTEG-1 film doped with 1 wt % n-DMBI exhibited a S of −690 μV/K. By furthering the n-DMBI loading, the S rapidly decreased in absolute value to −330 μV/K at 5 wt % and finally reached a plateau with more dopant. Similarly, the PTEG-1 film doped with TBAF showed a S of −606 μV/K at 2 wt %, which increased to −288 μV/K at 3 wt % and finally reached a regime with little change by further doping. The optimized $S^2\sigma$ of 16 and 24 μW/(m K^2) were achieved at doping concentrations of 5 and 3 wt % for n-DMBI and TBAF, respectively. Figure 5C

DOI: 10.1021/acsaem.9b01179
ACS Appl. Energy Mater. 2019, 2, 6664−6671

shows the S and $S^2\sigma$ of PTEG-1 film doped with Cs_2CO_3. In this scenario, the doping level of the PTEG-1 film can be modulated by the thickness of deposited Cs_2CO_3 layer. When the thickness of Cs_2CO_3 was 1 nm, the S was −286 μV/K, which decreased in absolute value to −212 μV/K with 8 nm thick Cs_2CO_3 layer. The smaller S of PTEG-1 films doped with Cs_2CO_3 than those obtained in the case of n-DMBI and TBAF doping indicates the higher doping level for the former. This explains the higher σ for PTEG-1-based film doped by Cs_2CO_3. Accordingly, the highest $S^2\sigma$ of 32 μW/(m K^2) was obtained, which is among the best n-type organic thermoelectrics (see Table 1).

3. CONCLUSIONS

To summarize, we studied the impact of different doping methods on the n-type thermoelectric properties of organic films. PTEG-1, with its characteristic polar side chain is used as the host, which is doped either by a one-step process with n-DMBI and TBAF as the dopant or by a two-step process with solid-state diffusion of Cs_2CO_3. Doping with Cs_2CO_3 gives the highest σ of ∼7.5 S/cm with the best $S^2\sigma$ of 32 μW/(m K^2) in this study, outperforming both the TBAF and n-DMBI-based systems. The PTEG-1 molecules stack into a bilayered architecture parrallel to the substrate. Cs_2CO_3 doping appears to exert the smallest influence on the spacing of the side chain plane likely due to its relatively small size compared with the other two. In a similar sense, PTEG-1 film doped by Cs_2CO_3 shows the highest density. Owing to these advantages, Cs_2CO_3-doped PTEG-1 film exhibits the best stability under a thermal stress (150 °C). The high power factor and good thermal stability of the PTEG-1/Cs_2CO_3 doping system make it very promising for tangible thermoelectric applications.

4. EXPERIMENTAL SECTION

4.1. Materials. PTEG-1 was synthesized by our group. TBAF, n-DMBI, and Cs_2CO_3 were purchased from Sigma-Aldrich.

4.2. Thermoelectric Characterization. Clean borosilicate glass substrates were treated with UV-ozone for 20 min. The doped films were spin-coated from a fullerene derivative solution (10 mg/mL in chloroform) blended with different amounts of dopant solution (20 mg/mL in chloroform) in a N_2-filled glovebox. The resultant films were subjected to thermal annealing at 120 °C for 1 h. The electrical conductivity measurements by four-point probes were performed in an N_2-controlled environment. The electrical conductivity was calculated with $\sigma = (I/V) \times L/(w \times d)$, with L (1 mm), w (4.5 mm), and d (100 nm) being the length, width, and height of the channel, respectively. The electrical conductivities of the separate points were averaged to obtain the electrical conductivity of one device. The Seebeck coefficients of doped PTEG-1 thin-film samples were measured in a home-built setup, as reported previously.[19] Two Peltier devices are placed with a gap of 6 mm in parallel on a heat sink. The temperatures of two Peltier devices can be controlled by two independent PID controllers (proportional−integral−derivative controllers). The two rectangular Au electrodes (width: 1.5 mm; length: 6 mm) are deposited on glass substrate with a distance of 6 mm. The large distance is used for avoiding the contact geometric effect. Two T-type thermocouples (127 μm from Omega) are used as probes for simultaneously temperature and thermal voltage. Note that a silver paste (ELECTRODAG 1415) was used to connect thermocouple probes with the Au electrodes. A Keithley 2000 mounted with scanner card is used for signal recording with a delay time of 100 ms. The system is controlled by Labview software. To remove the thermal voltage (ΔV) shifting, a "quasi-static" approach by slowly changing temperature difference (ΔT) is used to extract the Seebeck coefficient.

4.3. Microstructure Characterization. Grazing incidence wide-angle X-ray scattering (GIWAXS) measurements were performed using a MINA X-ray scattering instrument built on a Cu rotating anode source (λ = 1.5413 Å) by following the procedures reported previously.[45,46]

4.4. Optical Constant and Phase Behavior. The various PTEG-1-based films were prepared on clean silicon substrates with a thin layer of native oxide. The optical constants were measured by variable angle ellipsometry (J.A. Woollam Co., Inc). The Cauchy dispersion function was used for fitting to ellipsometry data to obtain refractive index in the transparent region. For the phase behavior measurement, the samples were placed in an air-protected sample holder filled with N_2, where variable temperature spectroscopic scan was performed (the incident angle of 70°). The film thickness variation with temperature was followed by using the previously reported procedure. Phase change leads to a change in volumetric expansion coefficient, which is directly translated into the tangent slope variation of $\rho-T$ function and hence the $d-T$ function.

■ ASSOCIATED CONTENT

Supporting Information

The Supporting Information is available free of charge on the ACS Publications website at DOI: 10.1021/acsaem.9b01179.

Figures S1−S3 (PDF)

■ AUTHOR INFORMATION

Corresponding Authors

*E-mail jian.liu@rug.nl.

*E-mail l.j.a.koster@rug.nl.

ORCID

Jian Liu: 0000-0002-6704-3895

Giuseppe Portale: 0000-0002-4903-3159

L. Jan Anton Koster: 0000-0002-6558-5295

Present Address

L.Q.: School of Materials Science and engineering, Yunnan Key Laboratory for Micro/Nano Materials & Technology, Yunnan University, 650091 Kunming, China.

Author Contributions

J.L. conceived this work. J.L. wrote the manuscript. M.P.G. and J.L. conducted the device fabrication and characterizations. J.D. and G.P. conducted microstructural characterization. B.Z. conducted ellipsometry test. L.Q. and J.C.H. provided the host material. J.L. and L.J.A.K. supervised this project. The manuscript was examined by all authors. The final manuscript was approved by all the coauthors.

Notes

The authors declare no competing financial interest.

■ ACKNOWLEDGMENTS

This work was supported by a grant from STW/NWO (VIDI 13476). This work is part of the research program of the Foundation of Fundamental Research on Matter (FOM), which is part of The Netherlands Organization for Scientific Research (NWO). This is a publication by the FOM Focus Group "Next Generation Organic Photovoltaics", participating in the Dutch Institute for Fundamental Energy Research (DIFFER). J.D. thanks the China Scholarship Council for the financial support.

■ REFERENCES

(1) Culebras, M.; Gómez, C.; Cantarero, A. Review on Polymers for Thermoelectric Applications. *Materials* **2014**, *7*, 6701−6732.

DOI: 10.1021/acsaem.9b01179
ACS Appl. Energy Mater. 2019, 2, 6664−6671

(2) Zebarjadi, M.; Esfarjani, K.; Dresselhaus, M. S.; Ren, Z. F.; Chen, G. Perspectives on Thermoelectrics: From Fundamentals to Device Applications. *Energy Environ. Sci.* **2012**, *5*, 5147−5162.
(3) Lu, N.; Li, L.; Liu, M. A Review of Carrier Thermoelectric-Transport Theory in Organic Semiconductors. *Phys. Chem. Chem. Phys.* **2016**, *18*, 19503−19525.
(4) Zhang, Q.; Sun, Y.; Xu, W.; Zhu, D. Organic Thermoelectric Materials: Emerging Green Energy Materials Converting Heat to Electricity Directly and Efficiently. *Adv. Mater.* **2014**, *26*, 6829−6851.
(5) Bell, L. E. Cooling, Heating, Generating Power, and Recovering Waste Heat with Thermoelectric Systems. *Science* **2008**, *321*, 1457−1461.
(6) Kroon, R.; Mengistie, D. A.; Kiefer, D.; Hynynen, J.; Ryan, J. D.; Yu, L.; Müller, C. Thermoelectric Plastics: From Design to Synthesis, Processing and Structure−Property Relationships. *Chem. Soc. Rev.* **2016**, *45*, 6147−6164.
(7) Russ, B.; Glaudell, A.; Urban, J. J.; Chabinyc, M. L.; Segalman, R. A. Organic Thermoelectric Materials for Energy Harvesting and Temperature Control. *Nat. Rev. Mater.* **2016**, *1*, 16050.
(8) Huang, D.; Yao, H.; Cui, Y.; Zou, Y.; Zhang, F.; Wang, C.; Shen, H.; Jin, W.; Zhu, J.; Diao, Y.; Xu, W.; Di, C.; Zhu, D. Conjugated-Backbone Effect of Organic Small Molecules for n-Type Thermoelectric Materials with ZT over 0.2. *J. Am. Chem. Soc.* **2017**, *139*, 13013−13023.
(9) Bubnova, O.; Khan, Z. U.; Malti, A.; Braun, S.; Fahlman, M.; Berggren, M.; Crispin, X. Optimization of the Thermoelectric Figure of Merit in the Conducting Polymer Poly(3,4-Ethylenedioxythiophene). *Nat. Mater.* **2011**, *10*, 429−433.
(10) Kim, G.-H.; Shao, L.; Zhang, K.; Pipe, K. P. Engineered Doping of Organic Semiconductors for Enhanced Thermoelectric Efficiency. *Nat. Mater.* **2013**, *12*, 719−723.
(11) Schlitz, R. A.; Brunetti, F. G.; Glaudell, A. M.; Miller, P. L.; Brady, M. A.; Takacs, C. J.; Hawker, C. J.; Chabinyc, M. L. Solubility-Limited Extrinsic n-Type Doping of a High Electron Mobility Polymer for Thermoelectric Applications. *Adv. Mater.* **2014**, *26*, 2825−2830.
(12) Fan, Z.; Du, D.; Guan, X.; Ouyang, J. Polymer Films with Ultrahigh Thermoelectric Properties Arising from Significant Seebeck Coefficient Enhancement by Ion Accumulation on Surface. *Nano Energy* **2018**, *51*, 481−488.
(13) Fan, Z.; Li, P.; Du, D.; Ouyang, J. Significantly Enhanced Thermoelectric Properties of PEDOT:PSS Films through Sequential Post-Treatments with Common Acids and Bases. *Adv. Energy Mater.* **2017**, *7*, 1602116.
(14) Patel, S. N.; Glaudell, A. M.; Peterson, K. A.; Thomas, E. M.; O'Hara, K. A.; Lim, E.; Chabinyc, M. L. Morphology Controls the Thermoelectric Power Factor of a Doped Semiconducting Polymer. *Sci. Adv.* **2017**, *3*, No. e1700434.
(15) Torabi, S.; Liu, J.; Gordiichuk, P.; Herrmann, A.; Qiu, L.; Jahani, F.; Hummelen, J.; Koster, L. J. A. Deposition of LiF onto Films of Fullerene Derivatives Leads to Bulk Doping. *ACS Appl. Mater. Interfaces* **2016**, *8*, 22623−22628.
(16) Sumino, M.; Harada, K.; Ikeda, M.; Tanaka, S.; Miyazaki, K.; Adachi, C. Thermoelectric Properties of N-Type C60 Thin Films and Their Application in Organic Thermovoltaic Devices. *Appl. Phys. Lett.* **2011**, *99*, 093308.
(17) Wang, Y.; Nakano, M.; Michinobu, T.; Kiyota, Y.; Mori, T.; Takimiya, K. Naphthodithiophenediimide−Benzobisthiadiazole-Based Polymers: Versatile n-Type Materials for Field-Effect Transistors and Thermoelectric Devices. *Macromolecules* **2017**, *50*, 857−864.
(18) Liu, J.; Qiu, L.; Portale, G.; Torabi, S.; Stuart, M. C. A.; Qiu, X.; Koopmans, M.; Chiechi, R. C.; Hummelen, J. C.; Anton Koster, L. J. Side-Chain Effects on N-Type Organic Thermoelectrics: A Case Study of Fullerene Derivatives. *Nano Energy* **2018**, *52*, 183−191.
(19) Yang, C.-Y.; Jin, W.-L.; Wang, J.; Ding, Y.-F.; Nong, S.; Shi, K.; Lu, Y.; Dai, Y.-Z.; Zhuang, F.-D.; Lei, T.; Di, C.; Zhu, D. B.; Wang, J.-Y.; Pei, J. Enhancing the N-Type Conductivity and Thermoelectric Performance of Donor-Acceptor Copolymers through Donor Engineering. *Adv. Mater.* **2018**, *30*, 1802850.
(20) Liu, J.; Qiu, L.; Portale, G.; Koopmans, M.; ten Brink, G.; Hummelen, J. C.; Koster, L. J. A. N-Type Organic Thermoelectrics: Improved Power Factor by Tailoring Host-Dopant Miscibility. *Adv. Mater.* **2017**, *29*, 1701641.
(21) Shi, K.; Zhang, F.; Di, C.-A.; Yan, T.-W.; Zou, Y.; Zhou, X.; Zhu, D.; Wang, J.-Y.; Pei, J. Towards High Performance N-Type Thermoelectric Materials by Rational Modification of BDPPV Backbones. *J. Am. Chem. Soc.* **2015**, *137*, 6979−6982.
(22) Zhao, X.; Madan, D.; Cheng, Y.; Zhou, J.; Li, H.; Thon, S. M.; Bragg, A. E.; DeCoster, M. E.; Hopkins, P. E.; Katz, H. E. High Conductivity and Electron-Transfer Validation in an n-Type Fluoride-Anion-Doped Polymer for Thermoelectrics in Air. *Adv. Mater.* **2017**, *29*, 1606928.
(23) Wang, S.; Sun, H.; Erdmann, T.; Wang, G.; Fazzi, D.; Lappan, U.; Puttisong, Y.; Chen, Z.; Berggren, M.; Crispin, X.; Kiriy, A.; Voit, B.; Marks, T. J.; Fabiano, S.; Facchetti, A. A Chemically Doped Naphthalenediimide-Bithiazole Polymer for n-Type Organic Thermoelectrics. *Adv. Mater.* **2018**, *30*, 1801898.
(24) Liu, J.; Ye, G.; van der Zee, B.; Dong, J.; Qiu, X.; Liu, Y.; Portale, G.; Chiechi, R. C.; Koster, L. J. A. N-Type Organic Thermoelectrics of Donor-Acceptor Copolymers: Improved Power Factor by Molecular Tailoring of the Density of States. *Adv. Mater.* **2018**, *30*, 1804290.
(25) Shin, Y.; Massetti, M.; Komber, H.; Biskup, T.; Nava, D.; Lanzani, G.; Caironi, M.; Sommer, M. Improving Miscibility of a Naphthalene Diimide-Bithiophene Copolymer with n-Type Dopants through the Incorporation of "Kinked" Monomers. *Adv. Electron. Mater.* **2018**, *4*, 1700581.
(26) Perry, E. E.; Chiu, C.-Y.; Moudgil, K.; Schlitz, R. A.; Takacs, C. J.; O'Hara, K. A.; Labram, J. G.; Glaudell, A. M.; Sherman, J. B.; Barlow, S.; Hawker, C. J.; Marder, S. R.; Chabinyc, M. L. High Conductivity in a Nonplanar *n* -Doped Ambipolar Semiconducting Polymer. *Chem. Mater.* **2017**, *29*, 9742−9750.
(27) Liu, J.; Qiu, L.; Alessandri, R.; Qiu, X.; Portale, G.; Dong, J.; Talsma, W.; Ye, G.; Sengrian, A. A.; Souza, P. C. T.; Loi, M. A.; Chiechi, R. C.; Marrink, S. J.; Hummelen, J. C.; Koster, L. J. A. Enhancing Molecular N-Type Doping of Donor-Acceptor Copolymers by Tailoring Side Chains. *Adv. Mater.* **2018**, *30*, 1704630.
(28) Kiefer, D.; Giovannitti, A.; Sun, H.; Biskup, T.; Hofmann, A.; Koopmans, M.; Cendra, C.; Weber, S.; Anton Koster, L. J.; Olsson, E.; Rivnay, J.; Fabiano, S.; McCulloch, I.; Müller, C. Enhanced N-Doping Efficiency of a Naphthalenediimide-Based Copolymer through Polar Side Chains for Organic Thermoelectrics. *ACS Energy Lett.* **2018**, *3*, 278−285.
(29) Liu, J.; Shi, Y.; Dong, J.; Nugraha, M. I.; Qiu, X.; Su, M.; Chiechi, R. C.; Baran, D.; Portale, G.; Guo, X.; Koster, L. J. A. Overcoming Coulomb Interaction Improves Free-Charge Generation and Thermoelectric Properties for n-Doped Conjugated Polymers. *ACS Energy Lett.* **2019**, *4*, 1556−1564.
(30) Han, G.; Popuri, S. R.; Greer, H. F.; Bos, J.-W. G.; Zhou, W.; Knox, A. R.; Montecucco, A.; Siviter, J.; Man, E. A.; Macauley, M.; Paul, D. J.; Li, W.-g.; Paul, M. C.; Gao, M.; Sweet, T.; Freer, R.; Azough, F.; Baig, H.; Sellami, N.; Mallick, T. K.; Gregory, D. H. Facile Surfactant-Free Synthesis of p-Type SnSe Nanoplates with Exceptional Thermoelectric Power Factors. *Angew. Chem.* **2016**, *128*, 6543−6547.
(31) Kroon, R.; Kiefer, D.; Stegerer, D.; Yu, L.; Sommer, M.; Müller, C. Polar Side Chains Enhance Processability, Electrical Conductivity, and Thermal Stability of a Molecularly p-Doped Polythiophene. *Adv. Mater.* **2017**, *29*, 1700930.
(32) Liu, J.; Maity, S.; Roosloot, N.; Qiu, X.; Qiu, L.; Chiechi, R. C.; Hummelen, J. C.; von Hauff, E.; Koster, L. J. A. The Effect of Electrostatic Interaction on N-Type Doping Efficiency of Fullerene Derivatives. *Adv. Electron. Mater.* **2019**, 1800959.
(33) Liu, J.; Li, X.; Zhang, S.; Ren, X.; Cheng, J.; Zhu, L.; Zhang, D.; Huo, L.; Hou, J.; Choy, W. C. H. Synergic Effects of Randomly Aligned SWCNT Mesh and Self-Assembled Molecule Layer for High-

DOI: 10.1021/acsaem.9b01179
ACS Appl. Energy Mater. 2019, 2, 6664−6671

Performance, Low-Bandgap, Polymer Solar Cells with Fast Charge Extraction. *Adv. Mater. Interfaces* **2015**, *2*, 1500324.
(34) Wolfe, R. M. W.; Menon, A. K.; Fletcher, T. R.; Marder, S. R.; Reynolds, J. R.; Yee, S. K. Simultaneous Enhancement in Electrical Conductivity and Thermopower of N-Type NiETT/PVDF Composite Films by Annealing. *Adv. Funct. Mater.* **2018**, *28*, 1803275.
(35) Zuo, G.; Li, Z.; Wang, E.; Kemerink, M. High Seebeck Coefficient and Power Factor in N-Type Organic Thermoelectrics. *Adv. Electron. Mater.* **2018**, *4*, 1700501.
(36) Qiu, L.; Liu, J.; Alessandri, R.; Qiu, X.; Koopmans, M.; Havenith, R. W. A.; Marrink, S. J.; Chiechi, R. C.; Anton Koster, L. J.; Hummelen, J. C. Enhancing Doping Efficiency by Improving Host-Dopant Miscibility for Fullerene-Based n-Type Thermoelectrics. *J. Mater. Chem. A* **2017**, *5*, 21234−21241.
(37) Li, C.-Z.; Chueh, C.-C.; Ding, F.; Yip, H.-L.; Liang, P.-W.; Li, X.; Jen, A. K.-Y. Doping of Fullerenes via Anion-Induced Electron Transfer and Its Implication for Surfactant Facilitated High Performance Polymer Solar Cells. *Adv. Mater.* **2013**, *25*, 4425−4430.
(38) Briere, T. R.; Sommer, A. H. Low-work-function Surfaces Produced by Cesium Carbonate Decomposition. *J. Appl. Phys.* **1977**, *48*, 3547−3550.
(39) Kang, K.; Watanabe, S.; Broch, K.; Sepe, A.; Brown, A.; Nasrallah, I.; Nikolka, M.; Fei, Z.; Heeney, M.; Matsumoto, D.; Marumoto, K.; Tanaka, H.; Kuroda, S.; Sirringhaus, H. 2D Coherent Charge Transport in Highly Ordered Conducting Polymers Doped by Solid State Diffusion. *Nat. Mater.* **2016**, *15*, 896−902.
(40) Campoy-Quiles, M.; Alonso, M. I.; Bradley, D. D. C.; Richter, L. J. Advanced Ellipsometric Characterization of Conjugated Polymer Films. *Adv. Funct. Mater.* **2014**, *24*, 2116−2134.
(41) Müller, C.; Bergqvist, J.; Vandewal, K.; Tvingstedt, K.; Anselmo, A. S.; Magnusson, R.; Alonso, M. I.; Moons, E.; Arwin, H.; Campoy-Quiles, M.; Inganas, O. Phase Behaviour of Liquid-Crystalline Polymer/Fullerene Organic Photovoltaic Blends: Thermal Stability and Miscibility. *J. Mater. Chem.* **2011**, *21*, 10676−10684.
(42) Cram, D. J.; Wilkinson, D. I. Macro Rings. XXIII. Carbonylchromium Complexes of Paracyclophanes and Model Compounds. *J. Am. Chem. Soc.* **1960**, *82*, 5721−5723.
(43) Lehn, J. M. Cryptates: The Chemistry of Macropolycyclic Inclusion Complexes. *Acc. Chem. Res.* **1978**, *11*, 49−57.
(44) Wang, S.; Sun, H.; Ail, U.; Vagin, M.; Persson, P. O. Å.; Andreasen, J. W.; Thiel, W.; Berggren, M.; Crispin, X.; Fazzi, D.; Fabiano, S. Thermoelectric Properties of Solution-Processed n-Doped Ladder-Type Conducting Polymers. *Adv. Mater.* **2016**, *28*, 10764−10771.
(45) Shao, S.; Dong, J.; Duim, H.; ten Brink, G. H.; Blake, G. R.; Portale, G.; Loi, M. A. Enhancing the Crystallinity and Perfecting the Orientation of Formamidinium Tin Iodide for Highly Efficient Sn-Based Perovskite Solar Cells. *Nano Energy* **2019**, *60*, 810−816.
(46) Shao, S.; Liu, J.; Fang, H.-H.; Qiu, L.; ten Brink, G. H.; Hummelen, J. C.; Koster, L. J. A.; Loi, M. A. Efficient Perovskite Solar Cells over a Broad Temperature Window: The Role of the Charge Carrier Extraction. *Adv. Energy Mater.* **2017**, *7*, 1701305.

DOI: 10.1021/acsaem.9b01179
ACS Appl. Energy Mater. 2019, 2, 6664−6671